

## The Impact of the New Island Divertor on the Plasma Performance in the W7-AS Stellarator

GRIGULL Peter, McCORMICK Kent, BURHENN Rainer, BRAKEL Rudolf, EHMLER Hartmut, FENG Yuehe, GADELMEIER Franz, GIANNONE Louis, HILDEBRANDT Dieter, JAENICKE Rolf, KISSLINGER Johann, KLINGER Thomas, KNAUER Jens, KOENIG Ralf, KUEHNER Georg, NAUJOKS Dirk, NIEDERMEYER Helmut, PASCH Ekkehard, RAMASUBRAMANIAN Narayanan, RUST Norbert, SARDEI Francesco, WAGNER Friedrich, WELLER Arthur, WENZEL Uwe  
and the W7-AS TEAM

*Max-Planck-Institut für Plasmaphysik, EURATOM Ass., D-85748 Garching, Germany*

(Received: 11 December 2001 / Accepted: 15 May 2002)

### Abstract

W7-AS has recently been equipped with ten open divertor modules in order to experimentally evaluate this exhaust concept in view of future application to W7-X. The new divertor enables access to a new NBI-heated, very high density (up to  $\bar{n}_e \approx 3.5 \times 10^{20} \text{ m}^{-3}$ ) operating regime with promising confinement properties. The energy confinement time increases steeply with density. In contrast, the particle and impurity confinement times decrease with increasing density. This allows full density control and stable quasi steady-state operation also under conditions of partial detachment from the divertor targets. Radiated power fractions are low to moderate in attached regimes and reach up to about 90% in detachment scenarios. The radiation mainly originates from lower ionization states of carbon and oxygen and stays always peaked at the edge.

### Keywords:

stellarator, W7-AS, improved confinement, steady-state, divertor

### 1. Introduction

Divertor solutions for stellarators have to be compatible with the specific edge configurations. One possibility is to utilize the flux diversion by inherent- or externally induced magnetic islands at the edge in order to establish edge plasma conditions and operational scenarios as achieved e.g. in tokamak poloidal field divertors. W7-AS is now being operated with such an (open) island divertor in order to experimentally evaluate this plasma exhaust concept in view of future application to W7-X. Initial efforts were focused mainly on the impact of the new divertor on the core plasma performance, on whether adequate boundary conditions at the upstream separatrix for high density divertor

operation can be achieved, and on the type of divertor scenarios which can be established with this geometry. First results have been published in ref. [1]. The present analysis gives an overview of the phenomenology and extends the parameter range studied.

### 2. Magnetic Field Configuration and Divertor Geometry in W7-AS

W7-AS is a modular stellarator with five magnetic field periods using non-planar field coils. The major and minor radii are  $R = 2 \text{ m}$  and  $a \leq 0.16 \text{ m}$ , respectively. The magnetic field strength at the axis is  $B \leq 2.5 \text{ T}$ . The plasma cross section per period varies from elliptical to

---

Corresponding author's e-mail: [grigull@ipp.mpg.de](mailto:grigull@ipp.mpg.de)

triangular and back to elliptical. The rotational transform  $\iota$  can be varied between 0.25 and 0.6 by currents in an additional set of planar coils; the magnetic shear is low. In cases with the local value of  $\iota_a = 5/m$  ( $m = 8, 9, 10\dots$ ) at the edge being resonant with the intrinsic  $B_{5,m}$  perturbation field component, the configurations are bound by macroscopic magnetic islands, which are utilized for the island divertor. The island topological parameters relevant for flux diversion can be varied within a broad range [1] by means of special control

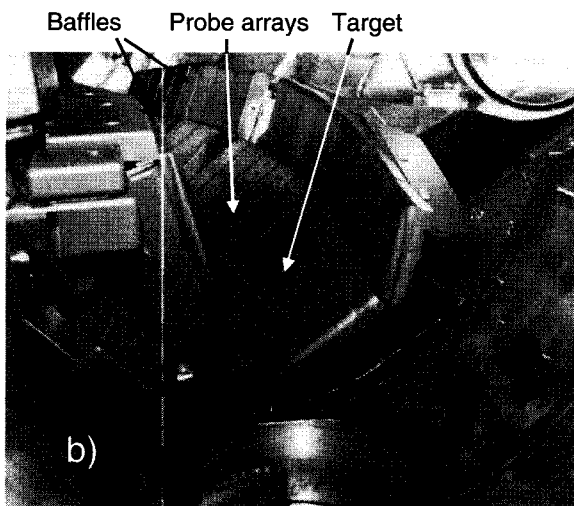
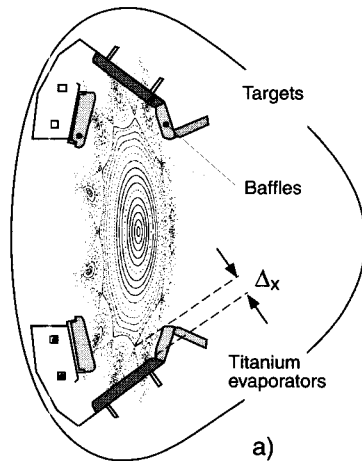


Fig. 1 (a) Elliptical plasma cross section with island divertor modules. Such modules are installed at the top and bottom of each of the five elliptical planes. The toroidal length of each module is 0.7 m.  $\Delta_x$  denotes the minimum separation between x-points and targets.

(b) Photograph of a bottom divertor module. The targets are made from CFC material, the baffles from isotropic fine-grain graphite.

coils affecting the  $B_{5,m}$  perturbation field magnitude. Present studies are performed at  $\iota_a = 5/9$  with a weak superimposed vertical field (100 G), which combination provides a good compromise between sufficiently large boundary islands and not too small main plasma cross sections.

The divertor consists of ten identical modules - two per field period - placed at the top and bottom of the elliptical cross sections, Fig. 1. Apart from the size, the geometry is similar in many aspects to that planned for W7-X [1,2]. Each module is composed of an inertially cooled target which intersects the islands, and of baffles for neutral control. Two thirds of the target tiles are instrumented with thermocouples; two opposite (top and bottom) modules are equipped with target-integrated, flush-mounted Langmuir probe arrays (for locations see further below).

### 3. Effects of the New Divertor

#### 3.1 Plasma performance at high density

The divertors enable access to a new NBI heated, very high density (up to  $\bar{n}_e \approx 3.5 \times 10^{20} \text{ m}^{-3}$ ) operating regime with promising confinement properties. Former high-power NBI discharges in W7-AS with limiters were mostly transient. Within the accessible density range of up to about  $2 \times 10^{20} \text{ m}^{-3}$ , the particle and impurity confinement times were rather long and increased with plasma density. The density could not be controlled, and both the density and the radiation from the core often quickly increased until the discharges collapsed. The density  $n_{es}$  at the upstream separatrix position increased less than linearly with the line-averaged density, and  $n_{es}$  values sufficiently high for favourable divertor regimes could be achieved only transiently [3]. This situation has completely changed in the new regime: above a certain threshold density, the energy confinement time  $\tau_E$  steeply increases, whereas, in contrast, the particle and impurity confinement times  $\tau_p$  and  $\tau_{imp}$  strongly decrease with increasing density. Consequently, high density, NBI-heated discharges, including discharges with partial detachment (see Sec. 3.2) from the divertor targets, can now be quasi-steadily maintained over many confinement times. Typical time traces of plasma parameters are shown in ref. [1]. The regime exhibits strong similarity to the quiescent H-mode [4], but avoids impurity accumulation. For that it is now termed High Density H-mode, HDH.

An overview of the existence range of the HDH regime in the configurational space studied so far is depicted in Fig. 2: Plotted are  $\tau_E$  contours for NBI

heated discharges (injected power  $P_{\text{NBI}} = 2$  MW, absorbed power  $P_{\text{NBI}}^{\text{abs}} = 1.4$  MW) as functions of the line-averaged density  $\bar{n}_e$  and the plasma minor radius  $a$  –varied by control coil currents– for separatrix-bounded configurations with  $t_a \approx 5/9$ . Increasing plasma radii correspond to decreasing minimum separations  $\Delta_x$  between x-points and targets (see Fig. 1a) and to decreasing radial widths of the magnetic islands. With the exception of the lowest densities, all data were

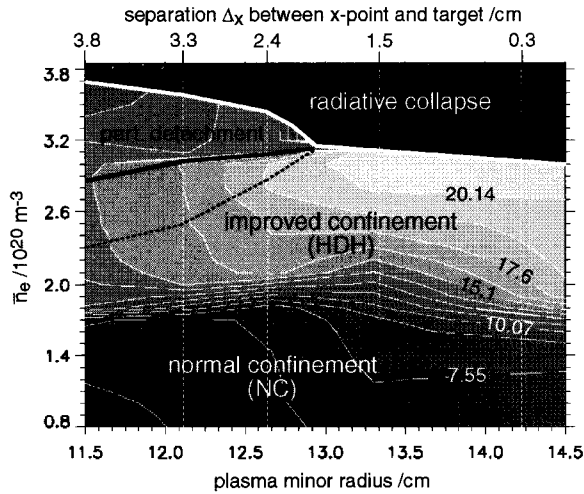


Fig. 2 Energy confinement times  $\tau_E$  [ms] for NBI discharges ( $P_{\text{NBI}}^{\text{abs}} = 1.4$  MW) as a function of the line-averaged density  $\bar{n}_e$  for various plasma minor radii (varied separation between x-points and targets, see Fig. 1a). The dashed black line indicates rollover of the particle flux over most of the target area (tiles 7–17, see Sec. 3.2).

obtained from quasi steady-state discharges. The steep increase of  $\tau_E$  with density at  $\bar{n}_e \approx 1.7 \times 10^{20} \text{ m}^{-3}$  is nearly independent of the magnetic configuration. For  $\Delta_x \geq 2.3$  cm and  $\bar{n}_e > 2.9\text{--}3.1 \times 10^{20} \text{ m}^{-3}$  partial detachment from the divertor targets is observed. With increasing  $\Delta_x$ , the onset of detachment shifts towards lower densities. Detachment extends the stable operation range to higher densities. Maximum densities exceed the GREENWALD limit [5] for an equivalent tokamak (elongation  $\kappa = 2$ , triangularity  $\delta = 0.3$ ) by a factor of about two. The degradation of  $\tau_E$  in detached regimes is moderate.

The subsequent analysis concentrates on discharges in the configuration with  $a = 11.5$  and  $\Delta_x = 3.9$  cm (Standard Divertor Configuration, SDC).

For attached HDH discharges, the  $\tau_E$  values lie well above relevant scalings, such as the W7-AS internal scaling (W7-95), the International Stellarator Scaling (ISS95), the New Large Helical Device scalings (NLHD1, NLHD2) and the Lackner Gottardi scaling (LGS) [6-8]. This is exemplarily shown in Fig. 3 for three different NBI heating powers ( $P_{\text{NBI}} = 1, 2$  and  $3.5$  MW,  $P_{\text{NBI}}^{\text{abs}} = 0.7, 1.4$  and  $2.5$  MW, respectively). The figure also demonstrates that –concomitant with the sudden jump of  $\tau_E$ – the impurity confinement time  $\tau_{\text{imp}}$  (measured by laser blow-off injection of aluminum) drastically decreases to values close to the energy confinement time. This favourable density dependence of  $\tau_{\text{imp}}$  is, as mentioned above, in strong contrast to previous experiments, which yielded a  $\tau_{\text{imp}} \propto n_e(0)^{1/2}/P^{0.8}$  scaling [9,10]. As a consequence, the impurity radiation from constant-density HDH discharges stays constant after the build-up phase of the discharges.

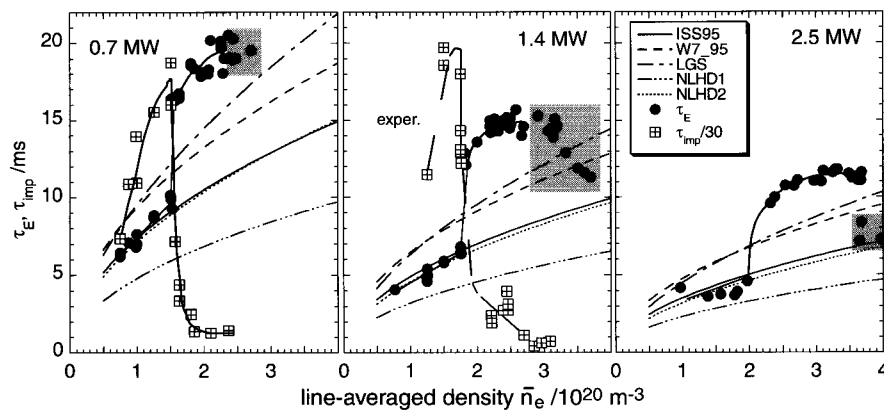


Fig. 3 Energy confinement times  $\tau_E$  and impurity confinement times  $\tau_{\text{imp}}$  (from laser blow-off injection of aluminum) as functions of the line-averaged density  $\bar{n}_e$  for NBI-heated discharges at different heating powers  $P_{\text{NBI}}^{\text{abs}}$  (Standard Divertor Configuration, SDC). Shaded ranges indicate partially detached discharges. Comparison of  $\tau_E$  with several scalings (see text).

Radiated power fractions  $f_r = P_{\text{rad}}/P_{\text{NBI}}^{\text{abs}}$  (with  $P_{\text{rad}}$  being the radiated power) are low to moderate but reach up to about 90% in detached discharges as shown in Fig. 4.

Radiative losses from normal confinement discharges at lower density are dominated by core radiation from higher ionization states of iron, oxygen and chlorine. Consistent with long impurity confinement times, the losses strongly increase with the discharge duration even in cases where the density can be kept fairly constant as demonstrated by radiated power density profiles (recorded by a 32 channel bolometer

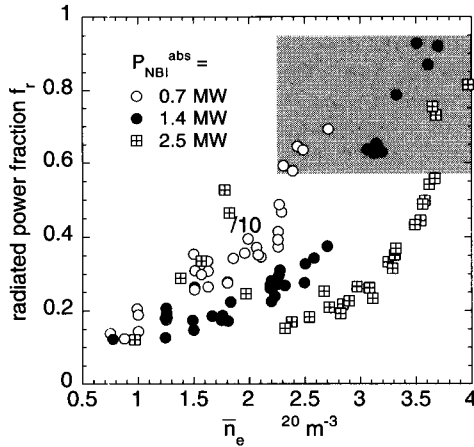


Fig. 4 Radiated power fractions  $f_r$  as functions of the line-averaged density  $\bar{n}_e$  for NBI-heated discharges (SDC). Gray shading indicates partially detached discharges.

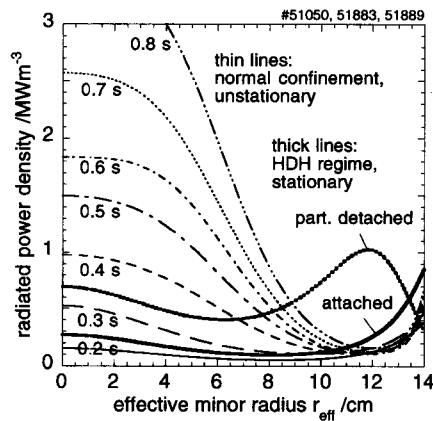


Fig. 5 Radiated power density profiles (from bolometer camera) for NBI heated discharges ( $P_{\text{NBI}}^{\text{abs}} = 1.4$  MW, SDC). Temporal evolution (thin lines) for a discharge with normal confinement at nearly constant  $\bar{n}_e \approx 1.7 \times 10^{20} \text{ m}^{-3}$ , and for stationary HDH discharges (thick lines) at  $\bar{n}_e = 2.4 \times 10^{20} \text{ m}^{-3}$  (attached) and  $3.2 \times 10^{20} \text{ m}^{-3}$  (partially detached).

camera) in Fig. 5. In contrast, the radiation in HDH discharges originates mainly from lower ionization states of carbon and oxygen and emanates always from near the edge. It should be noticed that the Abel inversion of the corresponding raw data could not treat the real island geometry at the edge. It was necessarily performed with the assumption that flux surfaces extend beyond the main plasma separatrix. Although local values from this radial range have to be taken with some care, the tendencies are clear. With 'stronger' detachment (increasing density and radiated power fraction), the raw data profiles become increasingly asymmetric, which could point towards a benign MARFE-like scenario.

With the transition from normal to HDH regimes, the  $n_e$  radial profiles typically change from centrally peaked to flat over most of the radius, with steep gradients at the edge, Fig. 6. The shape of the  $T_e$  profile does not significantly change. Based on these profiles, first SITAR code [11] simulations of the soft-X emission of aluminum (injected by laser blow-off) have been performed. They yielded nearly unchanged particle diffusion coefficients for the transition from normal to improved confinement, but a reduction of the inward convection velocity at the edge by factors of four to five.

Concomitant with broadened  $n_e$  profiles, the density  $n_{\text{es}}$  near the main plasma separatrix steeply increases to rather high values, which is an important pre-condition for favourable divertor operation, Fig. 7. With the

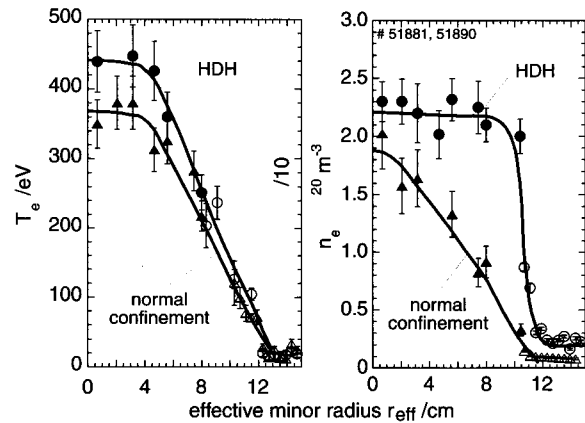


Fig. 6 Comparison of typical electron temperature  $T_e$  and density  $n_e$  radial profiles for NBI heated discharges ( $P_{\text{NBI}}^{\text{abs}} = 1.4$  MW, SDC) in the normal confinement and HDH regimes. The separatrix position is at  $r_{\text{eff}} \approx 11.5$  cm.

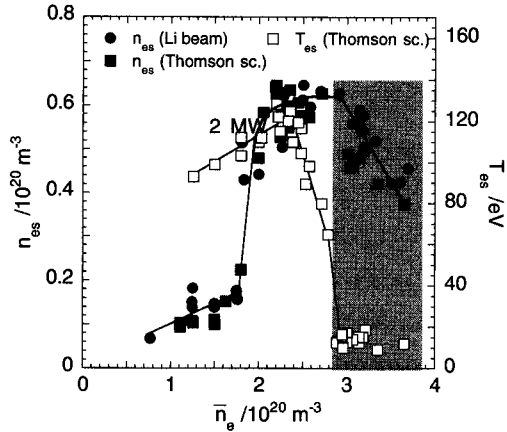


Fig. 7 Electron densities  $n_{es}$  (from Li beam and Thomson scattering) and temperatures  $T_{es}$  (from Thomson scattering) near the main plasma separatrix as functions of the line-averaged density  $\bar{n}_e$  ( $P_{NBI}^{abs} = 1.4$  MW, SDC). Lines are for guiding the eye only. The gray shaded range indicates partially detached discharges.

transition to partial detachment  $n_{es}$  shows rollover and decreases with increasing  $\bar{n}_e$ . Corresponding electron temperatures  $T_{es}$  (measured by Thomson scattering at the inboard side of a triangular cross section) typically start to decrease already at smaller  $\bar{n}_e$  values.

### 3.2 Divertor plasma regimes

The leading features of the divertor regimes were studied with diagnostics concentrated at two opposite (top and bottom) divertor modules. The interaction of the plasma with the targets typically concentrates mainly at two helical stripes. An example of  $H_\alpha$  patterns is shown in Fig. 8, in which the target tile and probe position terms used in the following are also defined. Within the strike zones, the thermal load typically shows strongest maxima at tile 12, which is closest to the main plasma, and at tiles further away from the main plasma but with steeper inclination to the field lines (tiles 5 or 6). Concerning rollover and detachment of the energy- and particle-fluxes,  $H_\alpha$ -, thermography- and Langmuir probe-data indicate a rather uniform behavior over most of the target plates (tiles 7–17, region D) with the exception of the ‘wing’ region (tiles 4–6, region A) which behaves differently. Downstream parameters measured with the probe array at tile 13 (representative for region D) are exemplarily shown in Fig. 9 which plots peak densities  $n_{ed}$  and temperatures  $T_{ed}$  versus  $\bar{n}_e$  for NBI (2 MW) discharges. With increasing  $\bar{n}_e$  the  $T_{ed}^{peak}$  values steadily decrease (as expected), and  $n_{ed}^{peak}$

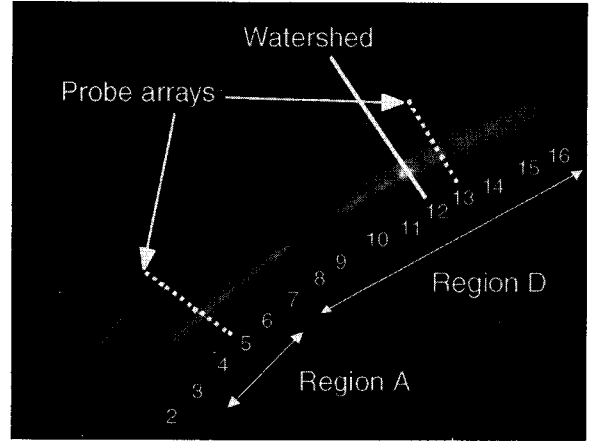


Fig. 8 View of a divertor target.  $H_\alpha$  traces show that interaction with the plasma is concentrated at two helical stripes. The numbers denote target tiles. The watershed (tile 12) is closest to the main plasma. The separation from the main plasma increases with increasing toroidal distance from tile 12. Tile 9 is slightly more retracted in order to allow diagnostic openings. Regions A and D show different features with respect to rollover and detachment (see text).

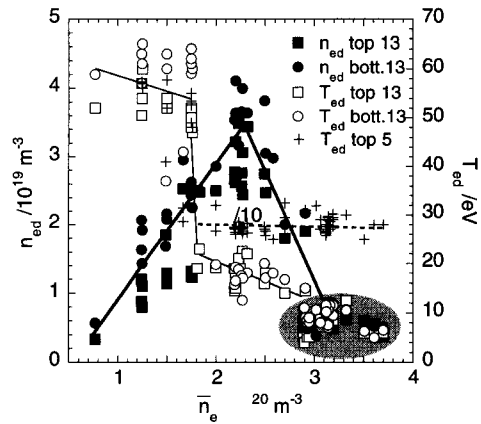


Fig. 9 Peak downstream densities  $n_{ed}$  and temperatures  $T_{ed}$  measured with the probe array at tile 13 (representative for target region D, see Fig. 8) for NBI discharges ( $P_{NBI}^{abs} = 1.4$  MW, SDC). The shaded area indicates detachment from region D. Peak temperatures measured at tile 5 (top target, region A) for comparison. Lines are for guiding the eye only.

exhibits –in agreement with  $H_\alpha$  data– rollover down to detachment. The threshold density for rollover increases with decreasing distance  $\Delta_x$  between x-points and targets (see Fig. 2). Rollover coincides with decreasing upstream temperature and, hence, decreasing upstream

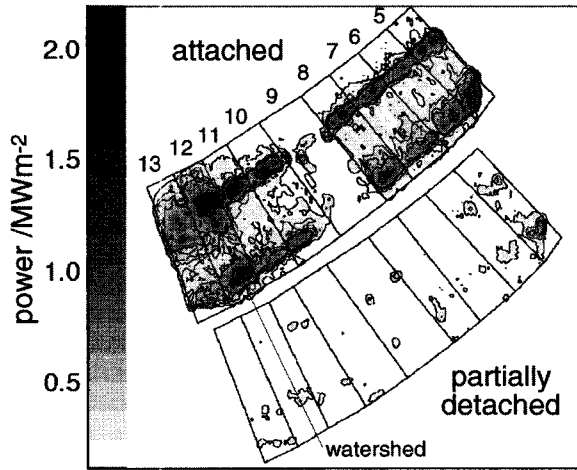


Fig. 10 Thermal load on a bottom target (from thermography) for attached and partially detached NBI discharges ( $P_{\text{NBI}}^{\text{abs}} = 1.4\text{MW}$ , SDC). The plasma at tile 5 stays attached during partial detachment, but at reduced thermal load.

plasma pressure. In contrast to tokamak divertors, it starts already at  $T_{\text{ed}} > 10$  eV where losses of parallel momentum by charge exchange neutrals are not expected to be efficient. Detachment from the strike zones is partial in the sense that the particle flux remains finite and  $T_{\text{ed}}$  stays above 2 eV (from  $H_{\alpha}/H_{\gamma}$  line intensities, not shown), where volume recombination is not yet effective. An important result is that the approach to this type of detachment is continuous. All intermediate states including partial detachment can be quasi-steadily maintained. One of the potentially stabilizing effects is that detachment is partial also in a spatial sense: the plasma in region A stays always attached, Fig. 10. Maximum temperatures and densities measured with probe arrays at tiles 5 (see ref. [1]) indicate a complex interplay between top and bottom targets, which changes with density and the level of the external gas feed; the peak temperatures stay, however, above 20 eV even at the highest density. This is inconsistent with the rather low upstream temperatures shown in Fig. 7 and could point again to an inhomogeneous temperature distribution near the separatrix and MARFE-like developments.

#### 4. Summary and Conclusion

W7-AS is operated with ten open divertor modules in order to experimentally evaluate this exhaust concept

in view of future application to W7-X. The divertor enables access to a new NBI heated, very high density operating regime with high energy- and low particle and impurity confinement times (HDH regime). This allows for full density control and stable quasi steady-state operation, also under conditions of partial detachment from the divertor targets. Radiated power fractions are low to moderate in attached regimes and reach up to about 90% in detachment scenarios. The radiation originates mainly from lower ionization states of carbon and oxygen and emanates always from the edge. The HDH regime is robust against changes of the magnetic field configuration, whereas stable detachment is restricted to configurations with sufficiently large clearances between x-points and targets. The physics background of the new regime is not yet clear, but a reduction of the inward pinch for impurities by flattening of the density profiles (due to broadened NBI deposition and strong recycling particle sources at the edge) seems to be a key ingredient. The access to the HDH regime is probably enabled by the strongly enlarged coverage of the plasma surface by carbon tiles which improves transient particle pumping and screens the plasma more efficiently from unfavourable interaction with the vessel wall.

#### References

- [1] P. Grigull *et al.*, accepted for publication in Plasma Phys. Control. Fusion **43** (2001).
- [2] H. Renner *et al.*, Nucl. Fusion **40**, 1083 (2000).
- [3] K. McCormick *et al.*, Plasma Phys. Control. Fusion **41**, B285-B304 (1999).
- [4] K. McCormick *et al.*, accepted for publication in PRL.
- [5] M. Greenwald *et al.*, Nucl. Fusion **28**, 2199 (1988).
- [6] U. Stroth *et al.*, Nucl. Fusion **36**, 1063 (1996).
- [7] K. Lackner and E. Gottardi, Nucl. Fusion **30**, 767 (1990).
- [8] K. Yamazaki *et al.*, IAEA Conf. on Fusion Energy, Sorrento, Italy, FTP2/12 (2000).
- [9] R. Burhenn *et al.*, Proc. 22<sup>nd</sup> Europ. Conf. on Contr. Fusion and Plasma Physics, Bournemouth, UK, 1995, Vol. **19c** Part III, p.145.
- [10] R. Burhenn *et al.*, Proc. 24<sup>th</sup> Europ. Conf. on Contr. Fusion and Plasma Physics, Berchtesgaden, Germany, 1997, Vol. **21a** Part IV, p.1609.
- [11] WVII-A Team, NI Group, Nucl. Fusion **25**, 1593 (1985).